Journal of Experimental Botany, Vol. 72, No. 10 pp. 3582–3596, 2021
doi:10.1093/jxb/erab087 Advance Access Publication 2 March, 2021

RESEARCH PAPER

Large-scale reconstruction of chromatin structures of maize temperate and tropical inbred lines

Lei Tian[1,2,3,*], Lixia Ku[1,2,*], Zan Yuan[4,*], Cuiling Wang[5], Huihui Su[1,2], Shunxi Wang[1,2], Xiaoheng Song[1,2], Dandan Dou[1,2], Zhenzhen Ren[1,2], Jinsheng Lai[6], Tao Liu[4,†], Chunguang Du[7,†] and Yanhui Chen[1,2,†]

[1] College of Agronomy, Henan Agricultural University, Zhengzhou 450002, China
[2] Synergetic Innovation Centre of Henan Grain Crops and National Key Laboratory of Wheat and Maize Crop Science, Zhengzhou 450002, China
[3] Henan Institute of Science and Technology for Development, Zhengzhou 450002, China
[4] Annoroad Gene Technology Co., Ltd, Beijing 100176, China
[5] College of Agronomy, Henan University of Science and Technology, Luoyang 471003, China
[6] State Key Laboratory of Agrobiotechnology and National Maize Improvement Center, Department of Plant Genetics and Breeding, China Agricultural University, Beijing 100193, China
[7] Department of Biology, Montclair State University, Montclair, NJ 07043, USA

* These authors contributed equally to this work
† Corresponding authors: chy9890@163.com; duc@montclair.edu or taoliu@genome.cn

Received 13 October 2020; Editorial decision 16 February 2021; Accepted 26 February 2021

Editor: Bjorn Usadel, Forschungszentrum Jülich, Germany

Abstract

Maize is a model plant species often used for genetics and genomics research because of its genetic diversity. There are prominent morphological, genetic, and epigenetic variations between tropical and temperate maize lines. However, the genome-wide chromatin conformations of these two maize types remain unexplored. We applied a Hi-C approach to compare the genome-wide chromatin interactions between temperate inbred line D132 and tropical line CML288. A reconstructed maize three-dimensional genome model revealed the spatial segregation of the global A and B compartments. The A compartments contain enriched genes and active epigenome marks, whereas the B compartments are gene-poor, transcriptionally silent chromatin regions. Whole-genome analyses indicated that the global A compartment content of CML288 was 3.12% lower than that of D132. Additionally, global and A/B sub-compartments were associated with differential gene expression and epigenetic changes between two inbred lines. About 25.3% of topologically associating domains (TADs) were determined to be associated with complex domain-level modifications that induced transcriptional changes, indicative of a large-scale reorganization of chromatin structures between the inbred maize lines. Furthermore, differences in chromatin interactions between the two lines correlated with epigenetic changes. These findings provide a solid foundation for the wider plant community to further investigate the genome-wide chromatin structures in other plant species.

Keywords: Chromatin structures, epigenetic change, Hi-C, large-scale reconstruction, maize germplasm, morphology, transcriptional regulation.

Abbreviations: Hi-C, high-resolution chromosome conformation capture; TADs, topologically associating domains; LD, long-day; SD, short-day; DEGs, differentially expressed genes; KEGG, Kyoto Encyclopaedia of Genes and Genomes; DBRs, differentially bound regions.

Introduction

The apparent randomness of chromatin packing during interphase is dynamically orchestrated to maintain gene expression, cell morphology, and physiological functions (Gibcus and Dekker, 2013). Three major models of three-dimensional (3D) spatial organization, Rabl, Rosette, and Bouquet, have been characterized based on the diversity in genome sizes, and have been explored using several imaging methods (Rodriguez-Granados *et al.*, 2016). The emergence of high-resolution chromosome conformation capture (Hi-C) technology has produced images with resolutions higher than those of previous microscopy-based analyses (Dekker *et al.*, 2002; Marella *et al.*, 2009; Schubert *et al.*, 2012). These enhanced images have led to more detailed and accurate investigations of the characteristics of chromosome architecture within the nucleus in various species, including yeast, animals, and plants (Zhang *et al.*, 2012; Mizuguchi *et al.*, 2015; Giorgetti *et al.*, 2016; Liu *et al.*, 2016; 2017). Chromosomal conformations are related to a genome-wide pattern of interactions involving two chromatin compartments, A and B, which are associated with genetic density, transcription levels, and the epigenetic landscape (Lieberman-Aiden *et al.*, 2009; Zhang *et al.*, 2012; Liu *et al.*, 2017). As basic structural and regulatory units, topologically associating domains (TADs) are stably maintained in distinct differentiated cells and tissues (Lieberman-Aiden *et al.*, 2009; Dixon *et al.*, 2012; Rao *et al.*, 2014; Sexton and Cavalli, 2015). The dynamic structure of genome-wide chromatin, including A/B compartment switching and TAD reorganization, can regulate the transcription level (Lupiáñez *et al.*, 2015; Giorgetti *et al.*, 2016). Recent technical developments have enabled researchers to examine genome-wide chromatin structures in mammals at the single-cell/nucleus level (Giorgetti *et al.*, 2016; Flyamer *et al.*, 2017). Despite rapid advances in the elucidation of chromatin structures in yeast and animal tissues, chromatin interactions have not been widely investigated in plants.

Our understanding of the genome-wide chromatin architecture in plants is mainly derived from a series of Hi-C analyses of the model plant species *Arabidopsis thaliana* (Wang *et al.*, 2015; Liu *et al.*, 2016). The *A. thaliana* chromosomes have simple interacting domains and alternating compact and loose structural domains that resemble the A and B compartments of mammals (Grob *et al.*, 2014). However, *A. thaliana* lacks prominent TADs at the genome level (Wang *et al.*, 2015). The Hi-C analyses of maize, tomato, sorghum, foxtail millet, and rice confirmed the existence of chromosomal A/B compartments (Dong *et al.*, 2017) and local distinct TADs in rice (Dong *et al.*, 2018). Additionally, Wang *et al.* (2017) uncovered large-scale chromatin interactions in upland cotton (*Gossypium hirsutum*). The rice single-cell 3D genomes (Zhou *et al.*, 2019) provide insights into the spatial arrangement of chromatin related to zygotic genome activation and epigenetic regulation in rice.

Chromosome conformation capture (3C) technologies have been used to examine chromatin 3D organization difference in different tissues or in the same tissue under different growth conditions (Liu *et al.*, 2017; Dong *et al.*, 2017; 2018; Wang *et al.*, 2018). A previous study reported chromosome decondensation in rice seedlings undergoing cold stress, despite local chromatin packing patterns remaining largely unchanged (Liu *et al.*, 2017). In addition, A/B compartment switching and TAD reorganization were observed between the sub-genomes of tetraploid cotton species and their putative diploid ancestors, thereby clarifying the effects of genome polyploidization on chromatin organization (Wang *et al.*, 2018). Recently, tissue-specific Hi-C maps of multiple plant species was constructed, unveiling the relationship between plant chromatin structural dynamics and transcription, as well as changes in epigenome features (Dong *et al.*, 2018; 2020).

Maize is a major crop cultivated worldwide and a model species for investigating genetics and genomics, partly because of its substantial genetic diversity (Hake and Ross-Ibarra, 2015). The single B73 genome might not be sufficient for exploring variations in genomic structures and spatial organization in maize. Hence, additional representative maize inbred lines are needed to fully capture the genome-wide chromatin organization. On the basis of its origin and evolution as well as the diversity in its responses to environmental conditions, particularly day length, maize germplasms can be divided into two major groups, temperate and tropical germplasms (Wu *et al.*, 2016). Under long-day (LD) conditions at high latitudes, tropical inbred lines flower very late or not at all, requiring adaptations to geographically and ecologically diverse local environments (Doebley, 2004). Considerable morphological differences between tropical and temperate inbred lines and the numerous underlying genes have been identified (Tian *et al.*, 2009), as have the differences in the genetics and epigenetics of tropical and temperate lines (Springer *et al.*, 2009; Mascheretti *et al.*, 2015). Recent studies have clarified the core structural features of chromatin organization, such as A/B compartments, TADs, and chromatin loops, in the inbred line B73 (Dong *et al.*, 2017; Li *et al.*, 2019; Peng *et al.*, 2019). A previous study reported the reduction of global B compartment interaction and local compartment partition in maize endosperm (Dong *et al.*, 2018). However, genome-wide chromatin conformations and spatial patterns among maize germplasms at different latitudes remain poorly characterized.

In this study, we applied Hi-C technology to reconstruct the 3D spatial organization of the chromosomal structures in a temperate line, D132, which is an elite Chinese maize inbred line, and in a tropical line, CML288, obtained from the International Maize and Wheat Improvement Center (CIMMYT, Mexico). By comparing the large-scale chromatin interactions of the D132 and CML288 inbred lines at a high resolution, we determined that approximately 8% of the genomes had undergone global compartmental transitions. A/B sub-compartment transition was also found to be associated with differential gene expression between two inbred

lines. Moreover, TAD reorganization and spatially separated A/B compartments were associated with 64% of the genomes, thereby influencing the transcriptional activity of many genes. Furthermore, differences in the histone modifications in distal regulatory regions may contribute to the diversity in the chromatin interactions of D132 and CML288. This study unveiled new genome structural differences between tropical and temperate maize inbred lines. The presented data may serve as a valuable resource for the wider plant community and may be used in future comparative analyses of genome-wide chromatin structures in other plant species.

Materials and methods

Plant materials

We acquired tropical maize inbred line CML288 from CIMMYT. Temperate inbred line D132 is a representative of the Chinese Reid heterotic group, which is a popular Chinese maize germplasm subpopulation (Wu *et al.*, 2014). The phenotypes of CML288 and D132 were observed under long day (LD) (Zhengzhou, 34°43′N, 113°43′E) and short day (SD; Sanya, 18°45′N, 109°30′E) in China. In the spring of 2016, we grew the two inbred lines in growth chambers (2.8×5.6×8.2 m) at 25 °C with a 16 h light/8 h dark photoperiod (light intensity of 100 μmol m^{-2} s^{-1}) in Zhengzhou, China. Leaves were collected from CML288 and D132 plants at the five fully expanded leaf stage for Hi-C, RNA-seq, and ChIP-seq analyses.

Hi-C library preparation

The fresh leaves were washed three times with sterile Milli-Q water, cut into pieces (approximately 1 mm^2), and transferred to 50 ml tubes containing 40 ml ice-cold 2% formaldehyde. Leaf samples were mixed by inverting the tubes at room temperature for 15 min. Next, 4.32 ml of 2.5 M glycine solution was added to quench the crosslinking reaction first at 25 °C for 5 min, and then on ice for 15 min. The material was filtered through four layers of Miracloth, ground into a fine powder in a chilled mortar filled with liquid nitrogen, and quickly transferred to 25 ml extraction buffer I [0.1 mM phenylmethylsulfonyl fluoride (PMSF), 10 mM Tris-HCl, pH 8, 0.4 M sucrose, 10 mM $MgCl_2$, 5 mM β-mercaptoethanol, and 1% protease inhibitor; Roche, Shanghai, China]. The solution was filtered and centrifuged at 5200 × *g* for 20 min at 4 °C, after which the pellet was resuspended in 1 ml extraction buffer II (0.1 mM PMSF, 10 mM Tris-HCl, pH 8, 0.25 M sucrose, 10 mM $MgCl_2$, 1% Triton X-100, 5 mM β-mercaptoethanol, and 1% protease inhibitor) on ice and centrifuged at 22000 × *g* for 10 min at 4 °C. The pellet was resuspended in 500 μl extraction buffer III (0.1 mM PMSF, 10 mM Tris-HCl, pH 8, 1.7 M sucrose, 2 mM $MgCl_2$, 0.15% Triton X-100, 5 mM β-mercaptoethanol, and 1 μl protease inhibitor), and then added to an equal amount of extraction buffer III before being centrifuged at 22000 × *g* for 10 min at 4 °C. The supernatant was carefully removed, after which 1 ml ice-cold cell lysis buffer [500 μl 10 mM Tris-HCl, pH 7.5, 10 mM NaCl, 0.2% NP-40 and 1× protease inhibitor cocktail (Roche)] was added and the samples were incubated on ice for 15 min.

The nuclei in cell lysis buffer were ground on ice with a cell homogenizer (slowly milled up and down 30 times). The cell suspension was transferred to a new Eppendorf tube and centrifuged at 2500 × *g* for 5 min at 4 °C. The supernatant was removed and the pellet was washed twice and resuspended in 500 μl ice-cold 1× CutSmart buffer. The solution was centrifuged at 2500 × *g* for 5 min at 4 °C. The nuclei were carefully resuspended and mixed in 0.01 ml 1× NEBuffer2. They were then solubilized with a 0.3% SDS solution and incubated at 65 °C for 10 min. After the SDS was quenched with Triton X-100, the samples were digested overnight with *Hind*III (400 units) at 37 °C on a rocking platform. The DNA ends were marked with biotin and the blunt end ligation of crosslinked fragments was induced by adding 1.5 μl 10 mM dA/T/GTP, 37.5 μl 0.4 mM biotin-14-dCTP, and 10 μl Klenow fragment to the tubes. The solution was mixed carefully and incubated at 37 °C for 45 min. After this, 86 μl of 10% SDS solution was added to inactivate the enzymes. The tubes were incubated at 65 °C for exactly 30 min and then immediately placed on ice. Next, 7.61 ml ligation mix [745 μl 10% Triton X-100, 745 μl 10× ligation buffer (500 mM Tris-HCl, pH 7.5, 100 mM $MgCl_2$, and 100 mM DTT), 80 μl of 10 mg ml^{-1} BSA, 80 μl of 100 mM ATP, and 5.96 ml water] was added to each tube, followed by gentle mixing and an incubation at 25 °C for 4–6 h.

The nuclei complexes were reverse-crosslinked during an incubation with proteinase K at 65 °C. The DNA was purified via phenol-chloroform extraction. Biotin-C was removed from the non-ligated fragment ends with T4 DNA polymerase. Smaller fragments ranging from 200 to 600 bp were generated by sonication. The fragment ends were repaired with a mixture of T4 DNA polymerase, T4 polynucleotide kinase, and Klenow fragment. The biotin-labelled Hi-C samples were specifically enriched with streptavidin C1 magnetic beads. The fragment ends were A-tailed with the Klenow fragment (exo−), after which the Illumina paired-end sequencing adapter ligation mix was added. Finally, the Hi-C libraries were amplified by 12–14 PCR cycles and sequenced with the Illumina HiSeq 4000 system. Each sample was analysed with three biological replicates, each comprising two technical replicates. The Pearson correlations between replicates are summarized in Supplementary Table S1 according to previous studies (Imakaev *et al.*, 2012; Servant *et al.*, 2015).

Read mapping and filtering

The low-quality reads were removed with fqtools_plus (https://github.com/annoroad/fqtools_plus) and the sequenced reads were truncated to 100 bp and mapped to the B73 RefGen_V4 genomic DNA sequence with Bowtie2 (version 2.2.3; Langmead and Salzberg, 2012). Read pairs within the same restriction enzyme fragments and PCR duplication were filtered with an optimized and flexible pipeline (HiC-Pro; Servant *et al.*, 2015). The high-quality alignments (MAPQ >10) were kept as previously described (Dong *et al.*, 2017). In the subsequent analysis, contact matrices were produced at all resolutions. Thus, we used a robust remove ICED (iterative correction and eigenvector decomposition) method with a multiplex bias (Servant *et al.*, 2015).

Hi-C data analysis

We generated two-dimensional heatmaps based on interaction frequency matrices. The interaction frequencies among multiple samples were compared following a direct subtraction of the *Z* score matrices.

Identification of A and B compartments

We analysed the global A compartment at a 1 Mb resolution, as previously described (Lieberman-Aiden *et al.*, 2009). Specifically, we used the matrix2 compartment module of the cworld online resource (https://github.com/dekkerlab/cworld-dekker). The expected score within the matrix was calculated with the Lowes smoothed average over the intra-chromosomal interactions. The observed/expected ratio was log_2-transformed for the final scores. Pearson correlations between normalized matrices were calculated, after which the correlation matrix was applied for a principal component analysis. The eigenvalue of the first principal component was then plotted as the compartment assignment, in which the positive value refers to a high gene density (A compartment or open chromatin), whereas bins with negative values are usually regions with

a low gene density (B compartment or closed chromatin). The gene density, guanine and cytosine (GC) and (transposable element) TE content were determined by calculating the number of genes and TEs in each bin according to the maize reference genes (B73 RefGen_V4). Maize B73 TE annotations were downloaded from "https://mcstitzer.github.io/maize_TEs/". The CscoreTool was used to call the sub-compartment for each block at 40 kb and 20 kb bin (Zheng and Zheng 2018).

Detection of topological domains

The Direction Index method was used to annotate the domains, as previously described (Dixon *et al.*, 2012). The TADs were calculated with 40 kb ICE-normalized matrices. For the pairwise TAD analysis, bedtools (https://bedtools.readthedocs.io/en/latest/) was used to calculate the proportion of overlapped TADs between two inbred lines. Merged and split TADs were defined as previously described (Ke *et al.*, 2017).

Enriched histone modification analysis

Five leaves of seedlings at the five-leaf stage in each inbred were pooled together for Chip-Seq. The histone ChIP-seq data were mapped to the B73 RefGen_V4 genome with Bowtie2. Peaks were called with the MACS software (version 2.1.2; https://pypi.org/project/MACS2/). The reads from the input sample were used as controls. The peaks were calculated for 10 kb bins in the genome. The enrichment score was calculated based on the $\log_2$ ratio of peak numbers over the window divided by the average of the genome-wide window, and plotted as line maps. Peaks were compared with the intersectBed program of bedtools (https://bedtools.readthedocs.io/en/latest/content/tools/intersect.html).

3D simulation

To clarify the chromosome structures in the nucleus, we modified a statistical approach using a Poisson distribution (PM1) method to convert the observed interactions into a 3D map with PASTIS software (Varoquaux *et al.*, 2014). To identify the global compartments in the 3D map, we calculated the actual distance by determining the Euclidean distance between each bin.

$$\text{Distance}\ (s1,\ s2) = \sqrt{(x_1 - x_2)^2 + (y_1 - y_2)^2 + (z_1 - z_2)^2}$$

Where s1, s2 indicate two bins given by PASTIS -PM1; x_1, y_1, and z_1 are the three-dimensional coordinates corresponding to s1; x_2, y_2, and z_2 are the three-dimensional coordinates corresponding to s2.

RNA-seq analysis

At the five fully expanded leaf stage, eight seedlings with an equal number of leaves were pooled for an RNA-seq analysis. Each genotype was analysed with three biological replicates. Total RNA was extracted with the RNeasy Plant Mini Kit (Qiagen, China). The sequencing libraries were constructed according to a standard protocol (Illumina, USA). We obtained approximately 25 million reads, after which the RNA-seq reads were aligned to the maize B73 RefGen_V4 genome sequence with the default parameters of TopHat (version 2.0.12; Trapnell *et al.*, 2012). The normalized RPKM (reads per kilobase per million mapped reads) values were calculated for each gene.

Differential chromatin interaction analysis

Significant intra-chromosomal interactions were identified with the Fit-Hi-C program (Ay *et al.*, 2014; multiple testing correction $P < 0.001$) at a 20 kb resolution. To run Fit-Hi-C, *Hind*III-digested fragments shorter than 2 kb were merged to construct chromosomal anchors. A differential interaction analysis was performed according to the MA-plot-based method with a random sampling model, as previously described (Li *et al.*, 2018).

Results

Characteristics of the genome-wide chromatin interactions in CML288 and D132

In this study, the phenotypes of CML288 and D132 differed greatly regarding plant architecture, development, and ear traits (Supplementary Table S2). In terms of field traits under short-day (SD) conditions, CML288 had more leaves and tassel branches, a thicker stem, and a greater plant and ear height, compared with D132 plants. An examination of the ear traits indicated that relative to the tropical maize line (CML288), the temperate maize inbred line (D132) had larger ears with a greater ear weight and produced more seeds and rows. There were also significant differences in the flowering times of CML288 and D132 under LD conditions. Specifically, CML288 tasselled 17 days later than D132 under LD conditions, and its reproduction was limited because of a lack of female floral development (Fig. 1A, B; Supplementary Table S2), indicating that the tropical maize line CML288 is extremely sensitive to the photoperiod under LD conditions.

To explore the genome-wide chromatin differences between CML288 and D132, we applied the Hi-C method to analyse these two maize inbred lines under LD conditions. Approximately 3.4 and 3.5 billion clean 100 bp paired-end reads were generated, of which 1.6 and 1.5 billion valid pairs were obtained for CML288 and D132, respectively (Supplementary Table S3). We then plotted the Hi-C map onto two-dimensional matrices that were normalized to megabase (Mb) sizes, to determine the interaction tendency between any two locations at the chromosomal level (Fig. 1C, D). The intra-chromosomal interactions were much stronger than the inter-chromosomal interactions in both maize lines. Moreover, intense interactions were detected among the pericentromeres and several telomeres (Fig. 1C, D), suggesting that pericentromeres may be located adjacent to one another within the nucleus, whereas several individual telomeres were randomly distributed in the nucleus, consistent with the results of the B73 inbred line (Supplementary Fig. S1), as described by Dong *et al.* (2017). The intra-chromosomal interactions along the anti-diagonal lines of chromosomes 9 and 10 appeared more frequently than the chromosome 1–4 contacts in both inbred lines (Fig. 1E, F; Supplementary Fig. S2), revealing the different levels of long-range interactions among 10 chromosomes. Furthermore, this study indicated that inter-chromosomal interactions were more frequent among large chromosomes (chromosomes 1–4 and 5) than between the smaller chromosomes in CML288 and D132, when considering B73 inbred lines (Fig. 1G, H, Supplementary Fig. S3).

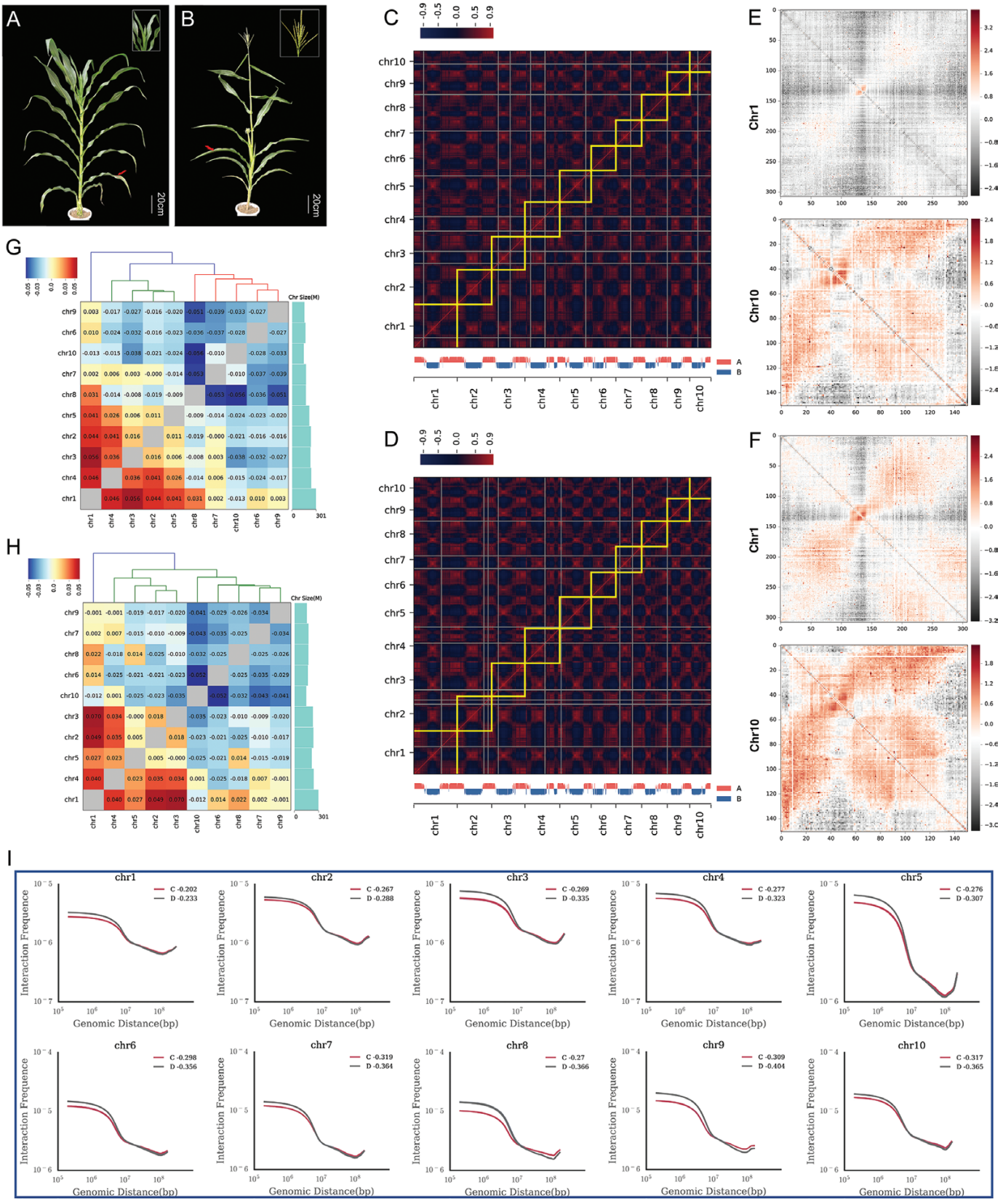

Fig. 1. Visualization of the Hi-C heatmaps of CML288 and D132. (A, B) Phenotypes of CML288 (A) and D132 (B) under LD conditions. The red arrow indicates the tenth leaves of CML288 and D132. (C, D) Genome-wide 2D interaction map of CML288 (C) and D132 (D) at a 1 Mb resolution. Ten chromosomes are presented from left to right and top to bottom. White-to-yellow-to-red indicates weak-to-strong interaction tendencies. (E, F) Enlarged

We also observed that chromosomes were differentially associated with each other between CML288 and D132. For example, chromosomes 1 and 5 were more closely associated with each other in D132 than in CML288. Overlaying the Hi-C matrices of CML288 and D132 plants revealed that for the same chromosomes, intra-chromosomal interactions (between 100 kb and 10 Mb) in CML288 were weaker than those in D132 (Fig. 1I). In particular, the reduction of chromatin contact intensity around the telomere regions is severe enough to be visible from their genome-wide Hi-C contact matrices (Supplementary Fig. S4A). The increasing contact intensity was found in the maize B73 inbred line when compared with both CML288 and D132 (Supplementary Fig. S4B, C). These results indicated distinct chromatin arrangements occurring in different maize inbred lines.

Global A/B compartment differences between CML288 and D132

The global A/B compartment differences between the two analysed maize lines were determined based on an eigenvector analysis of the genome-wide interaction matrix between CML288 and D132 (Lieberman-Aiden *et al.*, 2009). We identified global compartments A and B in the genome-wide chromatin (Fig. 2A), which was consistent with the reported findings for mammals and several other plant species (Lieberman-Aiden *et al.*, 2009; Zhang *et al.*, 2012; Dong *et al.*, 2017). The maize chromosomes adopt a simple structure with two A compartments at the chromosome tips and one continuous B compartment in the centre (Fig. 2A–E; Supplementary Fig. S5), consistent with the previous B73 results (Dong *et al.*, 2017; 2020). The global compartment pattern is consistent with the overall distribution pattern of euchromatin and heterochromatin in the maize chromosomes (Dong *et al.*, 2020). For example, approximately 80% of the maize genome is pericentromeric heterochromatin (global B compartment), and two euchromatin arms (global A compartment) are located at the distal ends (Meyers *et al.*, 2001). These results support the previously reported conclusion that the chromatin attraction and phase separation model might explain their formation (Dong *et al.*, 2020).

Furthermore, global A compartment content of CML288 was 3.12% lower than that of D132, implying that the spatial constraints were slightly less for CML288 than for D132. The global A compartment content of the 10 maize chromosomes was 35%–80.8% in CML288 and 39.6%–76.8% in D132 (Supplementary Table S4). The global A compartment represented 80.8% and 76.8% of chromosome 10 in CML288 and D132, respectively. In contrast, the global A compartment corresponded to only 35% of chromosome 7 in CML288, and 39.6% of chromosome 4 in D132 (Supplementary Table S4). Additionally, we determined that the differences in the global A compartment contents of chromosomes 5 and 7 between CML288 and D132 exceeded 4%. Specifically, the global A compartment contents of chromosomes 5 and 7 were 5.4% and 12% lower, respectively, in CML288 than in D132. The data indicated that the CML288 genome probably has a larger proportion of repressed chromatin than the D132 genome. Moreover, the global A compartment content of chromosome 10 was approximately 4% greater in CML288 than in D132. This increased content included a region with a global compartmental switch (chromosome 10: 92 000 000–93 000 000) and a large-effect quantitative trait locus (QTL) associated with photoperiod sensitivity (Supplementary Fig. S5). These results might be relevant for investigating biological processes, such as photoperiod sensitivity, and the variability in the chromatin states of tropical and temperate maize lines.

To explore the relationship between global A/B compartments and transcription as well as epigenetic feature, CML288 and D132 underwent an RNA-seq and Chip-seq analysis. A total of 6965 differentially expressed genes (DEGs) were identified, of which 3822 and 3143 exhibited down-regulated and up-regulated expression, respectively, in CML288 relative to the corresponding expression in D132 (Fig. 2F, G). Furthermore, the global A compartments in chromosome arms are associated with active epigenetic marks, and high transcription activity, whereas the global B compartment exhibited the opposite characteristics (Fig. 2H–K). To further sustain the segregation of the maize genome into two distinct compartments, we analysed the compartment structure in the global A and B compartment regions derived from the published Hi-C data of B73 maize inbred line (Dong *et al.*, 2017). A similar distribution pattern in B73 inbred line was found (Supplementary Fig. S6A), suggesting this global compartment partitioning is largely stable across different maize inbred lines. In addition, we found that four types of TEs showed distinct distributions between global A and B compartments, and GC content in individual chromosomes grouped in global A compartments also had a significantly different distribution (Wilcoxon rank sum test, $P<0.01$) compared with B compartments (Supplementary Fig. S6B, C). These results unveiled the relationship between global A/B compartments and TE distribution as well as GC content in maize. By comparing the genome-wide distribution of global A/B compartments in CML288 and D132, we determined that 51.16% and 40.08% of the global A and B compartments, respectively, were stable. Notably, of all global compartments, 8.76% differed between CML288 and D132

inter-chromosomal interaction heatmaps of chromosomes 1 and 10 in CML288 (E) and D132 (F). A colour axis is presented on the right. (G, H) Inter-chromosomal interactions between all pairs of chromosomes in CML288 (G) and D132 (H). Each block represents observed/expected interactions between chromosomes. Red and blue indicate enriched and depleted, respectively. Green bars on the right represent chromosome sequence lengths. Weak-to-strong interactions are indicated as blue-to-red. (I) Interaction decay exponents for CML288 and D132. Lines indicate the relative contact frequency of chromatin 0.1–100 Mb apart. C and D indicated CML288 and D132, respectively.

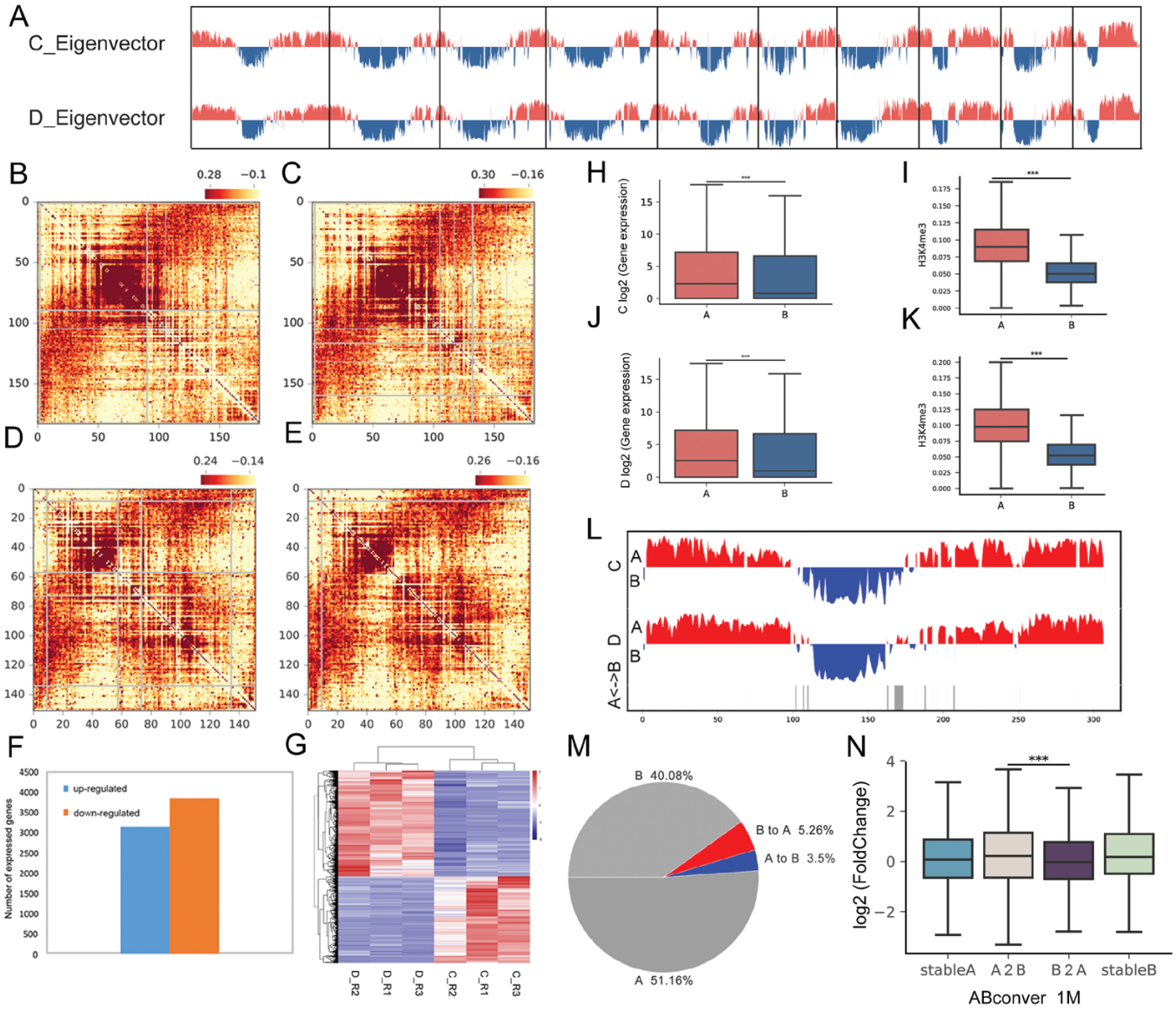

Fig. 2. Analysis of global A/B compartments and combined transcription and epigenetics feature between CML288 and D132. (A) Segregation of genome into global A/B compartments using genome-wide eigenvector in CML288 and D132. (B–E) Observed/expected heatmap revealing loci with either more or less (yellow) contacts than expected in chromosomes 7 (B, C) and 10 (D, E) of CML288 (B–D) and D132 (C–E). (F) Number of genes exhibiting up-regulated and down-regulated expression in CML288 relative to the expression in D132. (G) Heatmap of differentially expressed genes in CML288 and D132. C and D represented CML288 and D132; R1, R2, R3 indicate three biological replicates. (H–K) Distribution of gene expression values (H, J) and H3K4me3 level (I, K) in the global A/B compartments of CML288 (H, I) and D132 (J, K). ***P<0.001, Wilcoxon rank sum test. Y axis indicates the average of Log_2 (FPKM value) for three replicates of CML288 and D132. (L) First principal component of chromosome 1, representing the global A and B (blue) compartments. Grey bars represent the global compartmentalization differences between CML288 and D132. (M) Pie chart presenting the genomic compartment differences between the CML288 and D132 genomes. The stable global A and B compartments are presented in grey, whereas global B2A and A2B switches are indicated in red and blue, respectively. (N) D132/CML288 log_2 fold-change expression boxplot of all genes at specific regions for global compartmental switches. Genes associated with A2B (A compartments in CML288 that switched to B compartments in D132) and B2A (B compartments in CML288 that switched to A compartments in D132) exhibited significantly decreased and increased expression, respectively. ***P<0.001, Wilcoxon rank sum test.

(Fig. 2L, M; Supplementary Fig. S5; Supplementary Table S4). As expected, the CML288 up-regulated genes (778 of 1254 genes) were enriched in regions where the global B compartments in D132 transitioned to the global A compartments in CML288, whereas the opposite trend was observed for the down-regulated genes (Fig. 2N; Supplementary Table S5). These results implied that a decrease in the proportion of the global A compartment might be associated with some inhibited

genes in CML288. Furthermore, several of the enriched Kyoto Encyclopedia of Genes and Genomes (KEGG) pathways for the genes at global compartmental transition regions were related to stress responses or plant development, including 'biosynthesis of secondary metabolite', 'plant–pathogen interaction', and 'metabolic pathways' (Supplementary Table S6). These findings suggested that chromatin structural changes may closely link to the expression of genes involved in these biological pathways.

Reconstruction of the 3D spatial organization and spatial distribution of global A/B compartments in CML288 and D132

Genes separated by considerable distances at the genomic level can interact and function through long-range physical contacts (West and Fraser, 2005). Thus, clarifying the 3D spatial organization of the genome-wide chromatin is crucial for evaluating genome functions and genetic interactions as well as the underlying regulatory mechanisms. In the current study, the Hi-C data for two inbred lines were used to generate 3D whole-genome chromatin structures (Fig. 3A, B) based on Poisson methods (Varoquaux *et al.*, 2014). This 3D reconstruction revealed non-random chromosome conformations consistent with the chromosomal territories described by Cremer and Cremer (2010). We also examined the regions with global A/B compartments and observed that the global B compartments, including in the pericentromeric regions at the whole genome or individual chromosome levels, were spatially separated from the global A compartments, which clustered together at one pole of the nucleus near the nuclear envelope in both maize inbred lines (Fig. 3C, D; Supplementary Figs S7, S8). The interactions between the global A and B compartments were preliminarily characterized in different chromosomes in the two inbred lines (Fig. 3E–H). These results confirmed that distally located maize genomic regions or genes may frequently interact in 3D space.

To assess whether the conformation of the global A/B compartments was conserved among diverse plant species, we analysed published Hi-C data sets for rice and *A. thaliana* (Liu *et al.*, 2016; 2017). A similar 3D global compartmental arrangement at the nuclear pole was observed in *A. thaliana* (Fig. 3I;

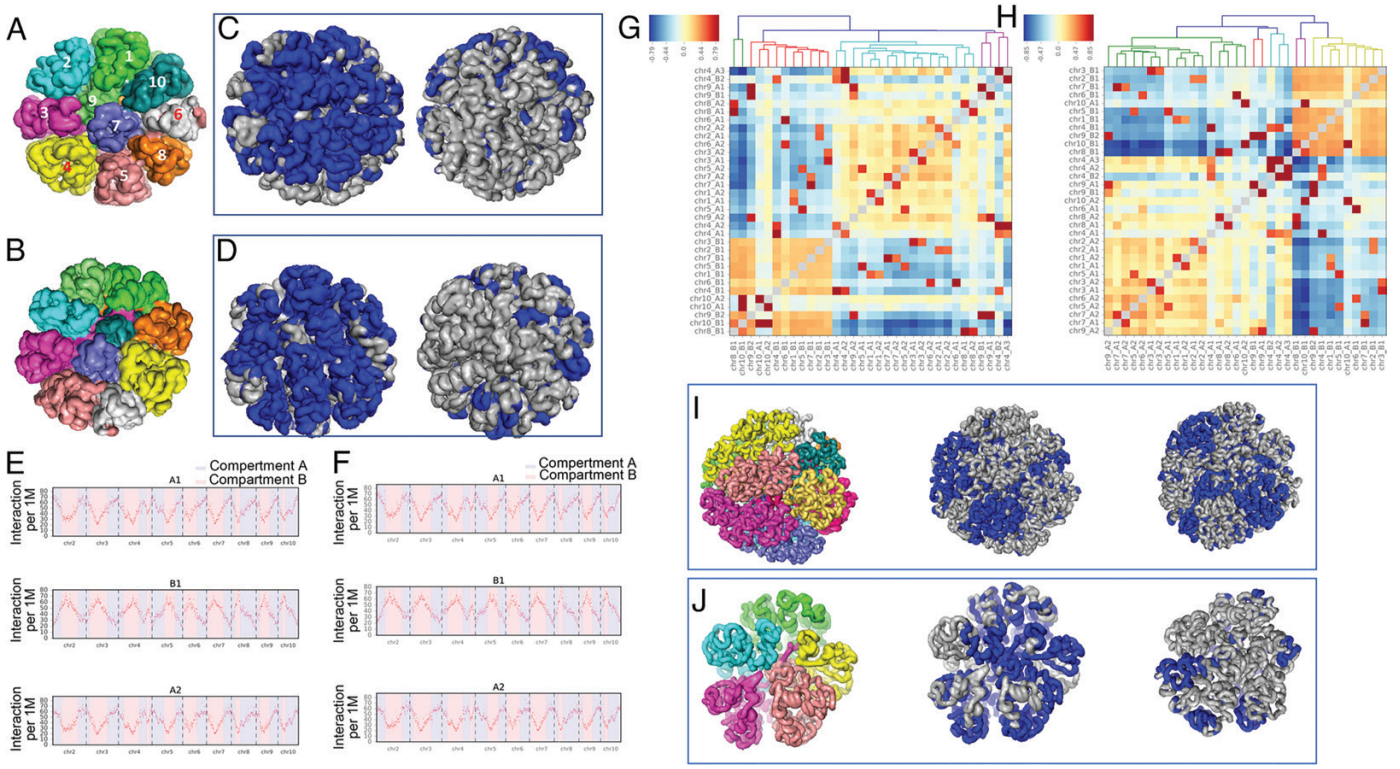

Fig. 3. Three dimensional structures of chromosomal contacts and the spatial distribution of global A/B compartments in maize, rice, and *Arabidopsis thaliana*. (A, B) Overall 3D structures of 10 maize chromosomes in CML288 (A) and D132 (B). Chromosomal territories are highlighted by different colours. (C, D) Spatial distribution of global A/B compartments in all chromosomes in CML288 (C) and D132 (D). The global A and B compartments are in blue and grey, respectively. The right image presents structures rotated by 180° relative to the structures in the left image. (E, F) Inter-chromosomal interactions of global A/B compartments between chromosome 1 and other chromosomes in CML288 (E) and D132 (F). (G, H) Cluster of inter-chromosomal interactions of global A compartment regions of chromosome 1 in CML288 (G) and D132 (H). (I, J) 3D structures of chromosomal contacts and the spatial distribution of A/B compartments in rice (I) *and A. thaliana* (J). Different chromosomal territories are indicated by different colours in the first image. The B and A compartments are presented in blue and grey, respectively, in the second and third images.

Supplementary Fig. S9), but not in rice (Fig. 3J; Supplementary Fig. S10). Additionally, a recent Hi-C study suggested that global A compartments in rice are located in the outer layer of the chromosomal territory (Liu *et al.*, 2017). The addition of our data to the published information may be useful for comparing the 3D genomic architecture of three plant species, and for highlighting the complexity of the 3D arrangement of chromatin in plant species with diverse genome sizes.

A/B sub-compartment dynamics associated with transcription

For large plant genomes, conventional A/B compartment partition methods are unable to separate the active gene islands from the largely inactive heterochromatin environment. It has been shown that large plant chromosomes could be further divided into A/B sub-compartments, also referred to as sub-compartments (Dong *et al.*, 2017; Doğan and Liu 2018). The CscoreTool was used to call sub-compartments for each block at 40 kb and 20 kb bins (Fig. 4A); the CscoreTool can more accurately detect the A and B compartments compared with principal component analysis (PCA)-based methods (Zheng and Zheng 2018). We examined whether A/B sub-compartments would display dynamic changes in two maize inbred lines (Fig. 4). Next, we inferred their active or repressive state using the normalized RNA-Seq read counts and histone modification in each bin. Regions classified as A sub-compartments are euchromatin regions with higher transcription activity and H3K4me3, compared with the B sub-compartments (Fig. 4B, C). We also showed that the inactive B to active A sub-compartment changes are indeed associated with transcriptional activation, while the A to B sub-compartment changes are associated with transcriptional repression (Fig. 4D–G). These results suggested that sub-compartment organization in two inbred lines could be linked to transcription.

Differences in the chromatin topology at the TAD level between CML288 and D132

During our examination of local chromatin domains, we detected 2348 and 2283 TADs in CML288 and D132, respectively, based on the methods of Dong *et al.* (2017). We detected a tight association between the TAD boundaries and gene expression. Specifically, genes closer to the TAD boundaries had

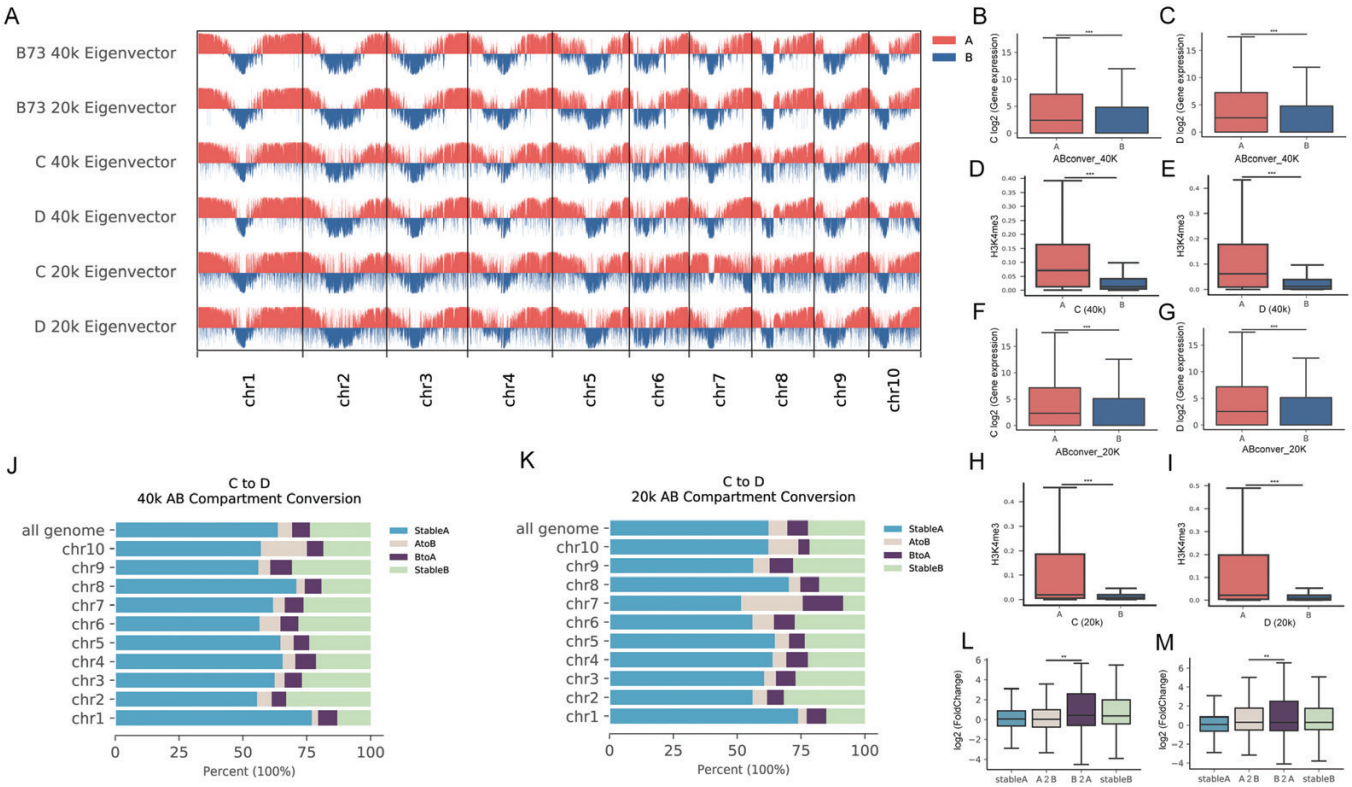

Fig. 4. A/B sub-compartments associated with transcription and epigenetics feature. (A) Segregation of genome into A/B sub-compartments in CML288 and D132 at 40 kb and 20 kb resolution. (B-E) Box plot showing regions that A/B sub-compartments are associated with gene expression and H3K4me3 accumulation at 40 kb resolution in CML288 (B, D) and D132 (C, E), respectively. (F-I) Box plots showing regions that A/B sub-compartments are associated with gene expression and H3K4me3 level at 20 kb resolution in CML288 (F, H) and D132 (G, I), respectively. (L-M) Switches from A to B sub-compartment in CML288 compared with D132 are associated with reduced RNA-Seq signal, and the switches from A to B sub-compartment are associated with increased RNA-Seq signal (***P*<0.01, ****P*<0.001, Wilcoxon rank sum test) at 40 kb (L) and 20 kb (M) resolution, respectively.

higher expression (Fig. 5A, B). Our investigation of domain-level changes for hierarchical TADs between CML288 and D132 uncovered four types of domain-level changes. By using D132 as a reference, we determined that 36% of the TADs were totally conserved, whereas 28.3% and 10.4% of the TADs were merged and split, respectively. The remaining 25.3% of TADs underwent complex domain-level changes in D132 (Fig. 5C). More than 60% of the TADs were involved in domain-level changes, which is a considerably higher percentage than that reported for the TAD reorganization between diploid and tetraploid cotton species (Wang *et al.*, 2018). Furthermore, we also observed a close relationship between domain changes and gene expression for merged and split TADs (Fig. 5D, E). These results indicated that large-scale changes to local chromatin organization occurred in D132 and CML288. The differences in chromatin structures may be due to the substantial genomic diversity between maize inbred lines. An earlier study confirmed that developmental transitions as well as biotic and abiotic stresses induce structural alterations to plant chromatin (Probst and Mittelsten Scheid, 2015). Thus, local environmental stress under LD conditions may lead to compartmental transitions in the SD-requiring tropical maize inbred line CML288.

Changes to intra-chromosomal interactions associated with altered H3K4me3 modifications in CML288 and D132

To compare the epigenetic states of CML288 and D132, we completed a ChIP-seq analysis with antibodies against H3K4me3 highly enriched in active promoters. A total of 67 126 and 43 541 H3K4me3 peaks were detected for CML288 and D132, respectively. By comparing the differentially bound regions (DBRs) in the two lines, we identified 2602 peaks for increased DBR density (gain peaks) and 3052 peaks for decreased DBR density (loss peaks) in CML288, relative to the peaks for D132 (Fig. 6A; Supplementary Table S7). Additionally, 2162 and 2415 genes were associated with the gain and loss DBRs, respectively. Of these gain and loss DBR genes, 514 and 548 were differentially expressed in CML288 and D132, respectively (Fig. 6B). The proportion of the genes

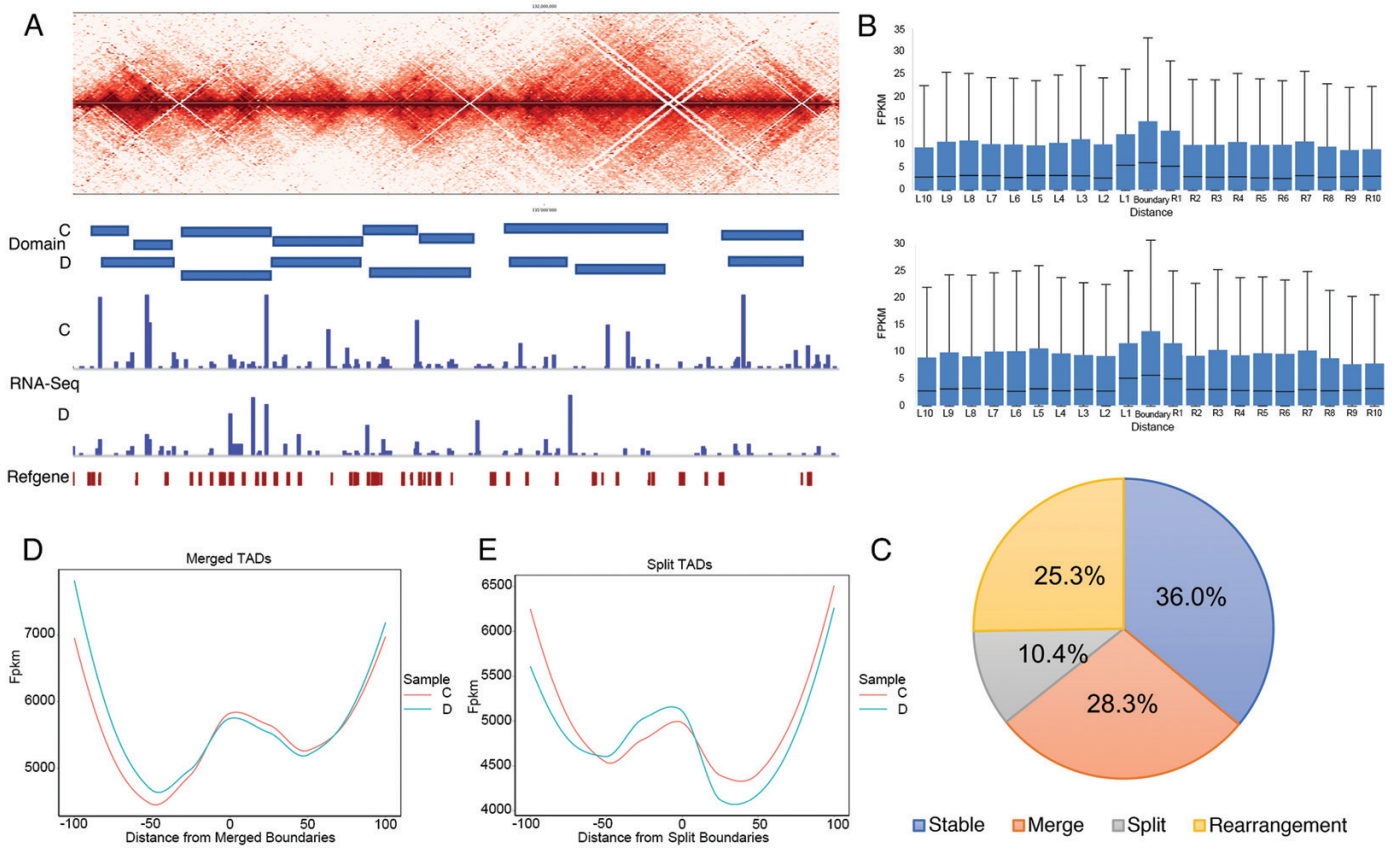

Fig. 5. Identification of maize topologically associating domains (TADs). (A) An example of TADs identified in part of chromosome 1 at a 40 kb resolution. (B) Gene expression around TAD boundaries in CML288 (upper panel) and D132 (lower panel). (C) Pie charts illustrating the proportion of hierarchical TAD changes, with D132 used as the reference. (D) Average gene expression at merged TADs around the merged boundaries. Merged TADs refer to two consecutive TADs in CML288 that merged to form a new TAD in D132. FPKM: fragments per kilobase of transcript per million fragments mapped. (E) Average gene expression at split TADs around the split boundaries. Split TADs refer to TADs in CML288 that split to form two consecutive TADs in D132.

related to DBRs that were differentially expressed between the two analysed maize lines was significantly higher (Fisher's exact test, $P<2.2e{-}16$) than the proportion of all genes that were differentially expressed between the two lines (44 474 total genes with 6965 DEGs). Thus, the gain and loss DBRs likely contributed to the detected up-regulated and down-regulated expression of the associated genes.

Histone modification states and transcriptional changes are reportedly correlated with chromatin interactions. To investigate this relationship, we identified 490 008 and 547 430 significant intra-chromosomal interactions (Benjamini-corrected, $P<0.01$). On the basis of the significant differences in the Hi-C contacts of CML288 and D132 (Benjamini-corrected $P<0.001$), 783 pairs of chromatin interactions with increased intensities (i.e. gain interactions) and 1330 pairs of chromatin interactions with decreased intensities (i.e. loss interactions; Fig. 6C) were identified. A comparison of the fold-changes in the H3K4me3 signals in the corresponding gene regions of the two inbred lines indicated that the histone signals significantly increased and decreased (Mann–Whitney U-test, $P<0.01$) for the gain and loss interactions, respectively (Fig. 6D). These findings implied that gene expression and H3K4me3 level is likely associated with most differences in the interactions between the two inbred lines. For example, several significant chromatin interactions were detected at the starting region of chromosome 8 in the two maize lines. Of these interactions, two pairs of gain interactions (chromosome 8: 1 080 000–1 100 000 and 1 140 000–1 160 000, $P<3.96e{-}13$; chromosome 8:

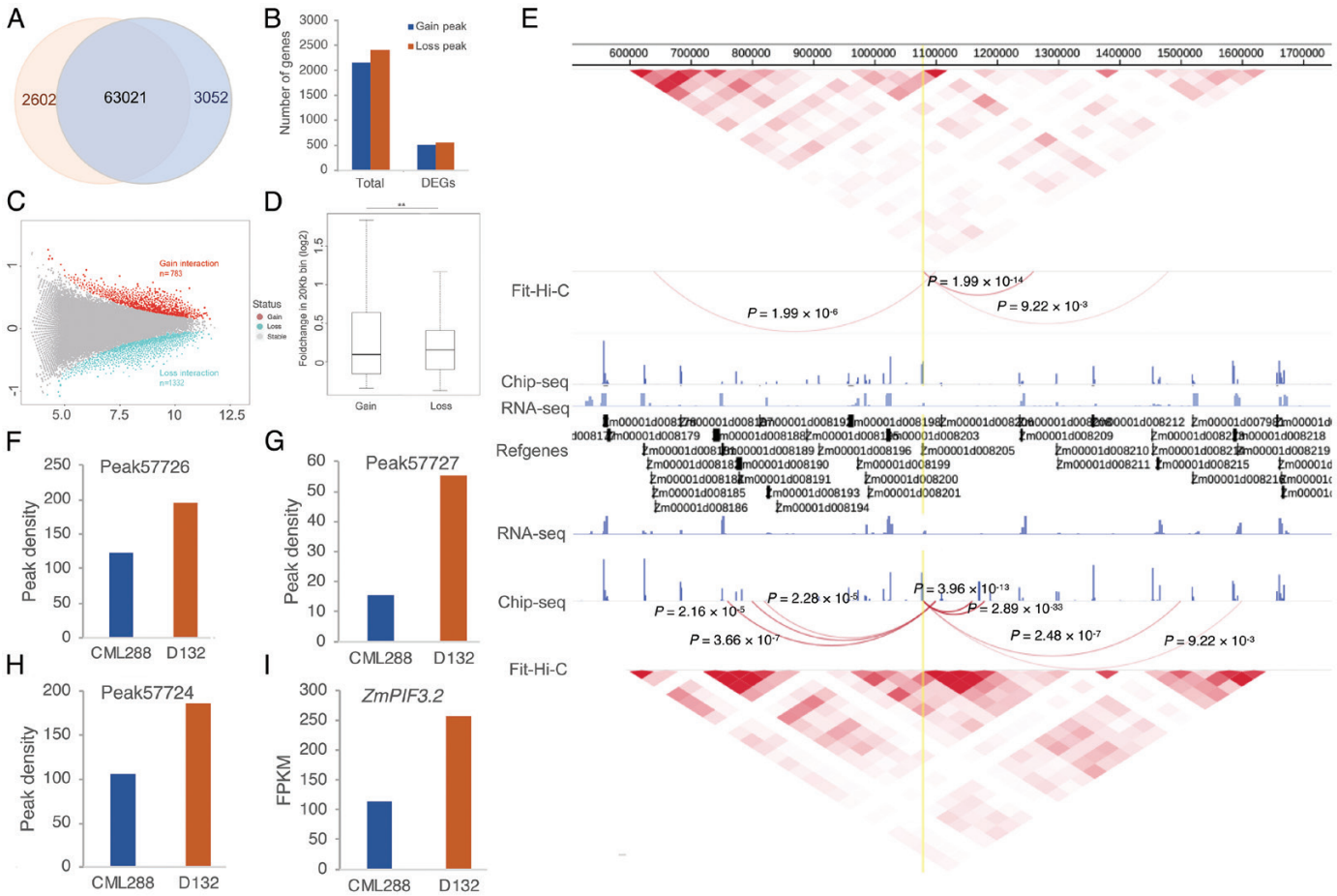

Fig. 6. Changes in histone modifications and chromatin interactions correlated with gene expression. (A) Venn diagram revealing the H3K4me3 peak overlap between CML288 and D132. (B) Number of differentially expressed genes associated with the gain and loss DBRs. (C) MA-plot for the differential interaction analysis. Red dots denote interactions with enhanced intensities in D132 compared with the interactions in CML288 (i.e. gain, Benjamini-corrected $P<0.01$). Cyan dots denote interactions with weakened intensities in CML288 (i.e. loss, Benjamini-corrected $P<0.01$). (D) Boxplot revealing that the H3K4me3 signal increased and decreased in gain and loss interactions, respectively, in D132. The *P* value was determined with the Mann–Whitney U-test: $^{**}P<0.001$. (E) Diagram presenting the ChIP-seq, RNA-seq, and Hi-C results for different chromatin interacting regions. Heatmap of Hi-C contacts in chromosome 8: 500 000:1 800 000, significant chromatin interactions, normalized H3K4me3 ChIP-seq coverage, and read coverage based on RNA-seq in CML288 (upper panel). Genome browser views of gene annotations (middle panel). Read coverage based on RNA-seq, normalized H3K4me3 ChIP-seq coverage, significant chromatin interactions, and a heatmap of Hi-C contacts in chromosome 8: 500 000:1 800 000 in D132 (lower panel). Only fragments with significant chromatin interactions are shown (multiple testing correction ,$^{**}P<0.01$). (F–H) Increased peak density in the gain DBRs in D132 relative to the levels in CML288. (I) Differences in the *ZmPIF3.2* FPKM values of maize inbred lines CML288 and D132.

1 080 000–1 100 000 and 1 160 000–1 180 000, $P<2.89e{-}33$) were detected in D132 (Fig. 6E). Consistent with these findings, we identified three H3K4me3 gain peaks corresponding to the interacting loci (Fig. 6F–H). Notably, the expression of the *Zm00001d008205* gene (*ZmPIF3.2* on chromosome 8: 1 080 000–1 100 000), which encodes a basic helix-loop-helix transcription factor, was significantly up-regulated in D132 (approximately 2.3-fold; Fig. 6I), suggesting that the gene may have a distinct regulatory function in D132, related to the long-range chromatin interaction.

Discussion

To date, Hi-C technology has been applied to compare tetraploid cotton species and their putative diploid ancestors, resulting in the first high-resolution characterization of the genome-wide chromatin architecture reorganization associated with biological processes in plants (Wang *et al.*, 2018). However, similar studies on other plant species have not been reported. Because of the substantial genetic and epigenetic diversity among maize germplasms, a Hi-C analysis of the genome of only one inbred line (e.g. B73) is insufficient for elucidating the genomic structure and spatial organization of the chromatin in maize. In the present study, we first confirmed the presence of global compartments and A/B sub-compartments, and local domains in the genomes of other maize inbred lines. Although principal components analysis is a descriptive statistical method for reducing dimensionality, the exact biological meaning of the compartment score is relatively elusive. For the large maize chromosomes, this method might not be biologically meaningful. In this study, we used the CscoreTool to call sub-compartments for each block at 40 kb and 20 kb bins; the CscoreTool can more accurately detect the A and B compartments than PCA-based methods (Zheng and Zheng, 2018). In addition, by performing higher-resolution chromosome conformation capturing methods such as *in situ* Hi-C or HiChIP (Ouyang *et al.*, 2020), compartments identified by conventional dilution Hi-C can be further segregated into different types of smaller compartmental domains or sub-compartments.

We also clarified the differences in the genome-wide chromatin interactions between the tropical maize inbred line CML288 and the temperate line D132. We uncovered a strong interaction along the primary diagonal and anti-diagonal lines in both CML288 and D132 (Fig. 1C-D), similar to the results of a recent study involving maize protoplasts, bundle sheath, mesophyll and endosperm (Dong *et al.*, 2017; 2020). The consistency in the results suggest that Hi-C analyses are stable across tissues. Thus, we compared our sequencing data with those in published reports, and analysed all of the previously generated raw sequencing data with the same parameter settings (Dong *et al.*, 2017). Our sequencing data generated more raw reads and valid Hi-C reads (approximately 3.3 billion and 1.5 billion reads, respectively) than the earlier investigation by Dong *et al.* (2017) where approximately 3 billion and 770 million reads were generated for raw reads and valid HiC reads, respectively.

The CML288 and D132 plants varied greatly in terms of architecture, ear traits, and development, especially in response to the photoperiod. The Hi-C analysis of CML288 and D132 in this study clarified the chromatin structures of these maize lines, including the A/B compartment switching and TAD reorganization. We determined that compared with D132, CML288 has 3.12% more global B compartments, and more genes with significantly down-regulated expression. Additionally, more than 8% of the genomes in the two maize lines were associated with global A/B compartment transitions with gene expression changes (Fig. 2). The enriched KEGG pathways associated with the corresponding genes were 'biosynthesis of secondary metabolite', 'plant–pathogen interaction', and 'metabolic pathways' (Supplementary Table S6), which affect plant development and stress responses. These results imply that global compartments switching between CML288 and D132 can be correlated with the expression changes of the genes involved in these pathways, ultimately resulting in the observed phenotypic differences between the two maize inbred lines. Among the phenotypic traits of tropical maize inbred lines grown under LD conditions, the photoperiod-dependent regulation of flowering is a major obstacle to the spread of maize from tropical regions to temperate locations (Buckler *et al.*, 2009). Notably, a global compartmental transition region (chromosome 10: 92 000 000–93 000 000) is associated with the well-characterized photoperiod sensitivity-related *qDPS10* locus (Supplementary Fig. S5). The region that comprises *qDPS10* is in bin 10.04 of maize chromosome 10, which includes several large-effect QTLs for local adaptation and domestication traits, accounting for 39.79%–44.30% of the phenotypic variance for the days-to-pollen shed under LD conditions (Tian *et al.*, 2009). This unexpected finding may help elucidate the photoperiod sensitivity at the whole-genome chromatin level. Future investigations of these altered chromatin regions may provide additional insights regarding the photoperiod sensitivity of maize.

In the current study, our Hi-C data revealed significant gain interactions in D132 near *ZmPIF3.2*. Moreover, up-regulated *ZmPIF3.2* expression was observed in the temperate inbred line (Fig. 6E-I). A recent study proved that *PIF3* helps integrate light and low-temperature signalling pathways (Lin *et al.*, 2018). Our results suggest that the higher *ZmPIF3* expression in D132 than in CML288 regulated by long-range chromatin interactions may mediate early flowering under LD conditions. However, the resolution of our Hi-C analysis is insufficient for detecting the regulatory elements and genes involved in chromatin looping. Thus, ChIA-PET, which is a site-specific chromosome conformation capture technique (Tang *et al.*, 2015), may be appropriate for high-resolution examination of small chromatin loops in plants.

We reconstructed the 3D spatial structures of the maize genome-wide chromatin based on Hi-C technology. The spatially segregated patterns of global A/B compartments in maize and *A. thaliana* were initially based on 3D models, consistent with previous related research on humans (Lieberman-Aiden *et al.*, 2009). However, the spatial distribution of global A/B compartments of the mid-sized rice genome differed from that of maize and *A. thaliana* (Fig. 3C, D, I, J). Accordingly, in plants, the spatial organization of chromosomes is not strictly related to genome size. With the technical development of chromosomal painting, the previous characterizations of chromosomal organization are somewhat rudimentary and possibly obsolete. For example, in *A. thaliana*, the chromatin was previously suggested to assume a Rosette-like conformation, but this has not been supported by subsequent fluorescence-based investigations, including FISH and Hi-C analyses (Schubert *et al.*, 2012; Grob *et al.*, 2014). This inconsistency may be caused by several factors, such as the existence and distribution of abundant repetitive genome sequences, as well as the dynamic chromatin properties, ploidy levels, and the associations with different nuclear structures (Schubert and Shaw, 2011). A limitation of our study is that the Hi-C experiments were performed using millions of cells as input. Therefore, the matrices and 3D models at the genome-wide level only represented the average of a population. Our data are insufficient for conclusively determining the 3D chromatin structural characteristics of individual cells.

Numerous previous studies have shown that chromatin 3D architecture is correlated with and underlies gene expression, and can cause developmental and pathogenic phenotypes (Bonev and Cavalli, 2016; Stam *et al.*, 2019). H3K4me3 is often described as an activating histone modification and chromatin activation mark, which are assumed to have an instructive role in the transcription of genes (Deal and Henikoff, 2011). Gene activity and epigenetic marks determine the activity level of the formed chromatin (Stam *et al.*, 2019). In this study, we mainly focused on the effect of differences in 3D chromatin architecture between two maize germplasms, on the gene expression associated with the histone H3K4me3 variations. The Hi-C differences between CML288 and d132 is also likely due to the other cues, such as genomic deletions, TE, repeat sequences, or DNA methylation variations. In addition, Hi-C data has been used to detect structural variants (Harewood *et al.*, 2017). When chromosomal rearrangements bring together distal regions of the same or different chromosomes, distinct blocks of what appear to be unusually strong long-range *cis* or *trans* interactions can be visible on the contact matrices (Harewood *et al.*, 2017). Hi-C has the ability to play a pivotal role in the detection of novel chromosomal abnormalities, both balanced and unbalanced, and the potential discovery of new fusion genes. Further use of Hi-C in this way and the generation of additional bioinformatic pipelines to analyse the data should cement the use of the technique for the detection of chromosomal rearrangements. However, the deletion of genome information of two inbred lines may also affect the Hi-C result and the subsequent structure analysis; thus more effort should be made to further validate the reasons that cause the chromatin difference, such as the completion of genome sequencing project of CML288 and D132.

Overall, our study revealed some basic similarities and differences between the tropical maize inbred line CML288 and the temperate line D132 at different chromosomal scales, from large-scale chromatin interactions to genomic compartmentalization and localized chromatin packing. Our findings may be useful in future studies on the regulatory effects of chromatin conformations on transcription as well as the growth and development of tropical and temperate inbred maize lines.

Supplementary data

The following supplementary data are available at *JXB* online.

Fig. S1. Pearson correlation matrix illustrating the correlation between the intra- and inter-chromosomal interaction profiles in B73 maize inbred line.

Fig. S2. Genome-wide 2D interaction map of CML288 and D132 at a 100 kb resolution for individual chromosomes.

Fig. S3. Inter-chromosomal interactions between all pairs of chromosomes in B73 maize inbred line.

Fig. S4. Genome-wide Hi-C contact maps of CML288 versus other lines.

Fig. S5. Translocation of global A/B compartments across tropical maize line CML288 and temperature maize line D132.

Fig. S6. Characteristics of the global A/B compartments in B73 maize inbred lines.

Fig. S7. The animations for 3D structures in CML288.

Fig. S8. The animations for 3D structures in D132.

Fig. S9. The animations for 3D structures in *A. thaliana*.

Fig. S10. The animations for 3D structures in rice.

Table S1. Pearson correlations between replicates in two maize inbred lines.

Table S2. Phenotypes of inbred CML288 and D132 lines under different photoperiod conditions.

Table S3. Number of reads based on the Hi-C data for CML288 and D132

Table S4. Percentage of global A/B compartments in each chromosome of CML288 and D132.

Table S5. RNA-seq analysis at the five-leaf stage in CML288 and D132.

Table S6. Enriched GO terms for genes located in the global A2B and B2A genomic regions.

Table S7. Gain and loss peaks identified between CML288 and D132.

Acknowledgements

We thank F. Han from the Chinese Academy of Sciences for critically reviewing this manuscript. We also thank Frasergen Bioinformatics Co., Ltd (Wuhan, China) for completing the bioinformatics analysis of TADs.

This study was financially supported by grants from the National Key Research and Development Program of China (2016YFD0101001) and the National Natural Science Foundation of China (31371628).

Conflict of interest

The authors have no conflict of interest to declare.

Author contributions

YC, CD, and LT conceived and designed the experiments; LK, LT, HS, SW and XS prepared the RNA-Seq and Hi-C library; LT, ZY, TL and SW performed the mapping and filtering of the Hi-C sequencing reads; ZY and TL analysed the ChIP-seq data; LK, CW, ZR, LT, HS and DD finished the RNA-Seq data analysis and QTL mapping; CD, LT, JL, and YC interpreted the data and drafted the manuscript with help from all the authors.

Data availability

The data that support the findings of this study are openly available in NCBI Sequence Read Archive (http://www.ncbi. nlm.nih.gov/sra/) under Accession number SRP44265.

References

Ay F, Bailey TL, Noble WS. 2014. Statistical confidence estimation for Hi-C data reveals regulatory chromatin contacts. Genome Research **24**, 999–1011.

Bonev B, Cavalli G. 2016. Organization and function of the 3D genome. Nature Reviews. Genetics **17**, 661–678.

Buckler ES, Holland JB, Bradbury PJ, *et al*. 2009. The genetic architecture of maize flowering time. Science **325**, 714–718.

Cremer T, Cremer M. 2010. Chromosome territories. Cold Spring Harbor Perspectives in Biology **2**, a003889.

Deal RB, Henikoff S. 2011. Histone variants and modifications in plant gene regulation. Current Opinion in Plant Biology **14**, 116–122.

Dekker J, Rippe K, Dekker M, Kleckner N. 2002. Capturing chromosome conformation. Science **295**, 1306–1311.

Dixon JR, Selvaraj S, Yue F, Kim A, Li Y, Shen Y, Hu M, Liu JS, Ren B. 2012. Topological domains in mammalian genomes identified by analysis of chromatin interactions. Nature **485**, 376–380.

Doebley J. 2004. The genetics of maize evolution. Annual Review of Genetics **38**, 37–59.

Doğan ES, Liu C. 2018. Three-dimensional chromatin packing and positioning of plant genomes. Nature Plants **4**, 521–529.

Dong P, Tu X, Chu PY, Lü P, Zhu N, Grierson D, Du B, Li P, Zhong S. 2017. 3D chromatin architecture of large plant genomes determined by local A/B compartments. Molecular Plant **10**, 1497–1509.

Dong P, Tu X, Li H, Zhang J, Grierson D, Li P, Zhong S. 2020. Tissue-specific Hi-C analyses of rice, foxtail millet and maize suggest non-canonical function of plant chromatin domains. Journal of Integrative Plant Biology **62**, 201–217.

Dong Q, Li N, Li X, *et al*. 2018. Genome-wide Hi-C analysis reveals extensive hierarchical chromatin interactions in rice. The Plant Journal **94**, 1141–1156.

Flyamer IM, Gassler J, Imakaev M, Brandão HB, Ulianov SV, Abdennur N, Razin SV, Mirny LA, Tachibana-Konwalski K. 2017. Single-nucleus Hi-C reveals unique chromatin reorganization at oocyte-to-zygote transition. Nature **544**, 110–114.

Gibcus JH, Dekker J. 2013. The hierarchy of the 3D genome. Molecular Cell **49**, 773–782.

Giorgetti L, Lajoie BR, Carter AC, *et al.* 2016. Structural organization of the inactive X chromosome in the mouse. Nature **535**, 575–579.

Grob S, Schmid MW, Grossniklaus U. 2014. Hi-C analysis in Arabidopsis identifies the KNOT, a structure with similarities to the flamenco locus of Drosophila. Molecular Cell **55**, 678–693.

Hake S, Ross-Ibarra J. 2015. Genetic, evolutionary and plant breeding insights from the domestication of maize. elife **4**, e05861.

Harewood L, Kishore K, Eldridge MD, Wingett S, Pearson D, Schoenfelder S, Collins VP, Fraser P. 2017. Hi-C as a tool for precise detection and characterisation of chromosomal rearrangements and copy number variation in human tumours. Genome Biology **18**, 125.

Imakaev M, Fudenberg G, McCord RP, Naumova N, Goloborodko A, Lajoie BR, Dekker J, Mirny LA. 2012. Iterative correction of Hi-C data reveals hallmarks of chromosome organization. Nature Methods **9**, 999–1003.

Ke Y, Xu Y, Chen X, *et al.* 2017. 3D chromatin structures of mature gametes and structural reprogramming during mammalian embryogenesis. Cell **170**, 367–381.e20.

Langmead B, Salzberg SL. 2012. Fast gapped-read alignment with Bowtie 2. Nature Methods **9**, 357–359.

Li E, Liu H, Huang L, Zhang X, Dong X, Song W, Zhao H, Lai J. 2019. Long-range interactions between proximal and distal regulatory regions in maize. Nature Communications **10**, 2633.

Li Y, He Y, Liang Z, *et al.* 2018. Alterations of specific chromatin conformation affect ATRA-induced leukemia cell differentiation. Cell Death & Disease **9**, 200.

Lieberman-Aiden E, van Berkum NL, Williams L, *et al*. 2009. Comprehensive mapping of long-range interactions reveals folding principles of the human genome. Science **326**, 289–293.

Lin L, Liu X, Yin R. 2018. PIF3 integrates light and low temperature signaling. Trends in Plant Science **23**, 93–95.

Liu C, Cheng YJ, Wang JW, Weigel D. 2017. Prominent topologically associated domains differentiate global chromatin packing in rice from Arabidopsis. Nature Plants **3**, 742–748.

Liu C, Wang C, Wang G, Becker C, Zaidem M, Weigel D. 2016. Genome-wide analysis of chromatin packing in *Arabidopsis thaliana* at single-gene resolution. Genome Research **26**, 1057–1068.

Lupiáñez DG, Kraft K, Heinrich V, *et al.* 2015. Disruptions of topological chromatin domains cause pathogenic rewiring of gene-enhancer interactions. Cell **161**, 1012–1025.

Marella NV, Malyavantham KS, Wang J, Matsui S, Liang P, Berezney R. 2009. Cytogenetic and cDNA microarray expression analysis of MCF10 human breast cancer progression cell lines. Cancer Research **69**, 5946–5953.

Mascheretti I, Turner K, Brivio RS, Hand A, Colasanti J, Rossi V. 2015. Florigen-encoding genes of day-neutral and photoperiod-sensitive maize are regulated by different chromatin modifications at the floral transition. Plant physiology **168**, 1351–1363.

Meyers BC, Tingey SV, Morgante M. 2001. Abundance, distribution, and transcriptional activity of repetitive elements in the maize genome. Genome Research **11**, 1660–1676.

Mizuguchi T, Barrowman J, Grewal SI. 2015. Chromosome domain architecture and dynamic organization of the fission yeast genome. FEBS Letters **589**, 2975–2986.

Ouyang W, Xiong D, Li G, Li X. 2020. Unraveling the 3D genome architecture in plants: present and future. Molecular Plant **13**, 1676–1693.

Peng Y, Xiong D, Zhao L, *et al.* 2019. Chromatin interaction maps reveal genetic regulation for quantitative traits in maize. Nature Communications **10**, 2632.

Probst AV, Mittelsten Scheid O. 2015. Stress-induced structural changes in plant chromatin. Current Opinion in Plant Biology **27**, 8–16.

Rao SS, Huntley MH, Durand NC, *et al.* 2014. A 3D map of the human genome at kilobase resolution reveals principles of chromatin looping. Cell **159**, 1665–1680.

Rodriguez-Granados NY, Ramirez-Prado JS, Veluchamy A, Latrasse D, Raynaud C, Crespi M, Ariel F, Benhamed M. 2016. Put your 3D glasses on: plant chromatin is on show. Journal of Experimental Botany **67**, 3205–3221.

Schubert I, Shaw P. 2011. Organization and dynamics of plant interphase chromosomes. Trends in Plant Science **16**, 273–281.

Schubert V, Berr A, Meister A. 2012. Interphase chromatin organisation in Arabidopsis nuclei: constraints versus randomness. Chromosoma **121**, 369–387.

Servant N, Varoquaux N, Lajoie BR, Viara E, Chen CJ, Vert JP, Heard E, Dekker J, Barillot E. 2015. HiC-Pro: an optimized and flexible pipeline for Hi-C data processing. Genome Biology **16**, 259.

Sexton T, Cavalli G. 2015. The role of chromosome domains in shaping the functional genome. Cell **160**, 1049–1059.

Springer NM, Ying K, Fu Y, *et al.* 2009. Maize inbreds exhibit high levels of copy number variation (CNV) and presence/absence variation (PAV) in genome content. PLoS Genetics **5**, e1000734.

Stam M, Tark-Dame M, Fransz P. 2019. 3D genome organization: a role for phase separation and loop extrusion? Current Opinion in Plant Biology **48**, 36–46.

Tang Z, Luo OJ, Li X, *et al.* 2015. CTCF-mediated human 3D genome architecture reveals chromatin topology for transcription. Cell **163**, 1611–1627.

Tian F, Stevens NM, Buckler ES 2009. Tracking footprints of maize domestication and evidence for a massive selective sweep on chromosome 10. Proceedings of the National Academy of Sciences, USA **106 Suppl 1**, 9979–9986.

Trapnell C, Roberts A, Goff L, Pertea G, Kim D, Kelley DR, Pimentel H, Salzberg SL, Rinn JL, Pachter L. 2012. Differential gene and transcript expression analysis of RNA-seq experiments with TopHat and Cufflinks. Nature Protocols **7**, 562–578.

Varoquaux N, Ay F, Noble WS, Vert JP. 2014. A statistical approach for inferring the 3D structure of the genome. Bioinformatics **30**, i26–i33.

Wang C, Liu C, Roqueiro D, Grimm D, Schwab R, Becker C, Lanz C, Weigel D. 2015. Genome-wide analysis of local chromatin packing in *Arabidopsis thaliana*. Genome Research **25**, 246–256.

Wang M, Tu L, Lin M, *et al.* 2017. Asymmetric subgenome selection and cis-regulatory divergence during cotton domestication. Nature Genetics **49**, 579–587.

Wang M, Wang P, Lin M, Ye Z, Li G, Tu L, Shen C, Li J, Yang Q, Zhang X. 2018. Evolutionary dynamics of 3D genome architecture following polyploidization in cotton. Nature Plants **4**, 90–97.

West AG, Fraser P. 2005. Remote control of gene transcription. Human Molecular Genetics **14 Spec No 1**, R101–R111.

Wu X, Li Y, Shi Y, Song Y, Wang T, Huang Y, Li Y. 2014. Fine genetic characterization of elite maize germplasm using high-throughput SNP genotyping. Theoretical and Applied Genetics **127**, 621–631.

Wu Y, San Vicente F, Huang K, *et al.* 2016. Molecular characterization of CIMMYT maize inbred lines with genotyping-by-sequencing SNPs. Theoretical and Applied Genetics **129**, 753–765.

Zhang Y, McCord RP, Ho YJ, Lajoie BR, Hildebrand DG, Simon AC, Becker MS, Alt FW, Dekker J. 2012. Spatial organization of the mouse genome and its role in recurrent chromosomal translocations. Cell **148**, 908–921.

Zheng X, Zheng Y. 2018. CscoreTool: fast Hi-C compartment analysis at high resolution. Bioinformatic **9**, 9.

Zhou S, Jiang W, Zhao Y, Zhou DX. 2019. Single-cell three-dimensional genome structures of rice gametes and unicellular zygotes. Nature Plants **5**, 795–800.